JOURNAL OF MATERIALS SCIENCE **36** (2001) 5593–5601

Effect of the microstructure on the mechanical properties of a directionally solidified $Y_3Al_5O_{12}/Al_2O_3$ eutectic fiber

D.-Y. PARK, J.-M. YANG
Department of Materials Science and Engineering, University of California, Los Angeles, CA 90095, USA
E-mail: jyang@seas.ucla.edu

The strength and fracture behaviors of a directionally solidified $Y_3Al_5O_{12}/Al_2O_3$ eutectic fiber were investigated. The fiber was grown continuously by an edge-defined film-fed growth (EFG) technique. The microstructure was characterized using X-ray diffraction (XRD), scanning electron microscopy (SEM), and energy dispersive spectroscopy (EDS). The room temperature tensile strength and Weibull's modulus of the eutectic fiber before and after heat treatment at 1460°C were measured. The fracture toughness and crack propagation behaviors were investigated using an indentation technique. Significant coarsening of the lamellar microstructure was observed after heat treatment at 1460°C in air. The degradation of the room temperature tensile strength in the $Y_3Al_5O_{12}/Al_2O_3$ eutectic fiber after heat treatment was attributed to the development of surface grooves at the surface of the fiber. Also, the $Y_3Al_5O_{12}/Al_2O_3$ eutectic fiber showed a radial (Palmqvist) crack type and exhibited an anisotropic crack propagation behavior during the indentation tests.

1. Introduction

Oxide-based fibers are the most promising materials as the reinforcing materials for high temperature structural applications in oxidizing environments because of their inherent thermal stability. As a result, several single-crystal oxide fibers (such as Al_2O_3, $MgAl_2O_4$, $Y_3Al_5O_{12}$ and Y_2O_3-stabilized ZrO_2) [1–4] and oxide-oxide eutectic fibers (such as $Y_3Al_5O_{12}/Al_2O_3$ and $Al_2O_3/ZrO_2(Y_2O_3)$) have been developed [5–8]. Among the single-crystal oxides and oxide-oxide eutectics, the directionally solidified $Y_3Al_5O_{12}/Al_2O_3$ eutectic system has been demonstrated as the most promising system due to its chemical, microstructural, mechanical, and thermal stability. It has been reported that the tensile strength of the $Y_3Al_5O_{12}/Al_2O_3$ eutectic fiber decreased with heat treatment at elevated temperature [9, 10]. However, the exact mechanisms leading to the decrease of tensile strength after heat treatment in the $Y_3Al_5O_{12}/Al_2O_3$ eutectic fiber have not yet been identified. As the diameter of the fiber become smaller, the change of the surface morphology and/or coarsening of the fine lamellar structure at high temperatures may affect the mechanical properties of the fiber.

Since Hertz first investigated the cone-shaped fracture at elastic contacts between glass lenses in 1896, indentation mechanics has become extensively used in the analysis and characterization of fracture and deformation properties of brittle ceramics [11, 12], as well as metals and other materials. Traditionally, Hertzian cone crack has been most widely studied in flat silicate glass plate, using sphere indenter of hard steel or tungsten carbide. Extensive studies to other brittle solids such as single crystals and hard, fine-grain polycrystalline ceramics become more prevalent in 1950s–1970s [12]. More recently, indentation tests with sharp indenters such as Vickers and Knoop indenters were developed in 1970s due to the geometrical similarity of the residual impressions; the contact pressure is independent of indent size, and thus affords a convenient measure of hardness [13]. Radial-median crack produced by diamond pyramid indenter is now the most widely used of all fracture testing methodologies in the mechanical evaluation of brittle materials.

The purpose of this work is to study the effect of microstructure on the mechanical properties and fracture behavior of the $Y_3Al_5O_{12}/Al_2O_3$ eutectic fiber.

2. Experimental procedure

The $Y_3Al_5O_{12}/Al_2O_3$ eutectic fibers produced by Saphikon Inc. (Milford, NH) with a nominal diameter of 75 μm were used in this study. The fibers were grown continuously using an EFG technique at a growth rate of 2.03 cm/min. A detailed description of the EFG process can be found elsewhere [14, 15]. X-ray diffractometer (Model 42202, Norelco, North American Phillips Company Inc.) with Cu K_α radiation was used for the identification of the phases in the fibers. Microstructures of the fiber at the surface, the interior section along

fiber axis (the longitudinal section) and the cross section areas were examined using a scanning electron microscope (Stereoscan 250, Cambridge, Scientific Instruments Ltd., Valencia, CA). Both the longitudinal section and the cross section areas to the fiber axis were polished to 0.1 μm diamond compounds finish. The backscattered electron image was used to identify the eutectic lamellar structure at the surface, the longitudinal section and the cross section areas of the fibers. The lamellar spacing was measured by a linear intercept method. Straight scanning lines were placed on SEM photos, rotated at 15° intervals from 0 to 165° due to the anisotropy of the lamellar microstructure [16]. Tensile strength at room temperature was measured using an Instron universal testing machine (Model 5544, Instron Corp., Canton, MA) with a crosshead speed of 0.127 mm/min. Fiber ends were mounted on tabs with epoxy for gripping. A gauge length of 2.54 cm was used. Prior to heat treatment and tensile test, all the fibers were ultrasonically cleaned. An indentation technique was conducted on the polished surface of the fiber to measure the fracture toughness and to study the crack growth behavior. Vickers hardness tester (Micromet II Microhardness Tester, Buhler Ltd., Lake Bluff, Illinois) was used to make a crack on the polished surface of the fiber. The cracks were generated under a load of 100 g and the crack lengths were measured using a SEM. The $Y_3Al_5O_{12}/Al_2O_3$ fiber with a nominal diameter of 75 μm could not sustain more than 100 g load.

3. Results

3.1. Microstructural evolution

The backscattered electron images of the as-fabricated fiber at the surface, the longitudinal section and the cross section areas are shown in Fig. 1. The three different areas (the surface, the longitudinal section and the cross section areas) are defined as shown in Fig. 1d. The lamellar eutectic microstructures of the as-fabricated fibers were clearly observed using the backscattered electron image due to the effect of the atomic number contrast between $Y_3Al_5O_{12}$ (YAG) and Al_2O_3 (alumina) phases. It is evident that the microstructure of the as-fabricated fiber consisted of fine lamellar microstructures with YAG phases (bright phase) distributed uniformly in alumina phase (dark phase). The lamellar spacing of the as-fabricated fibers for the surface, the longitudinal section and the cross section areas were measured to be 0.40 μm, 0.52 μm and 0.46 μm, respectively.

X-ray diffraction analysis indicated the fiber contained both $Y_3Al_5O_{12}$ and Al_2O_3 phases in the as-fabricated and the post-heat-treated states as shown in Fig. 2. Some SiO_2 peaks appeared after heat treatment

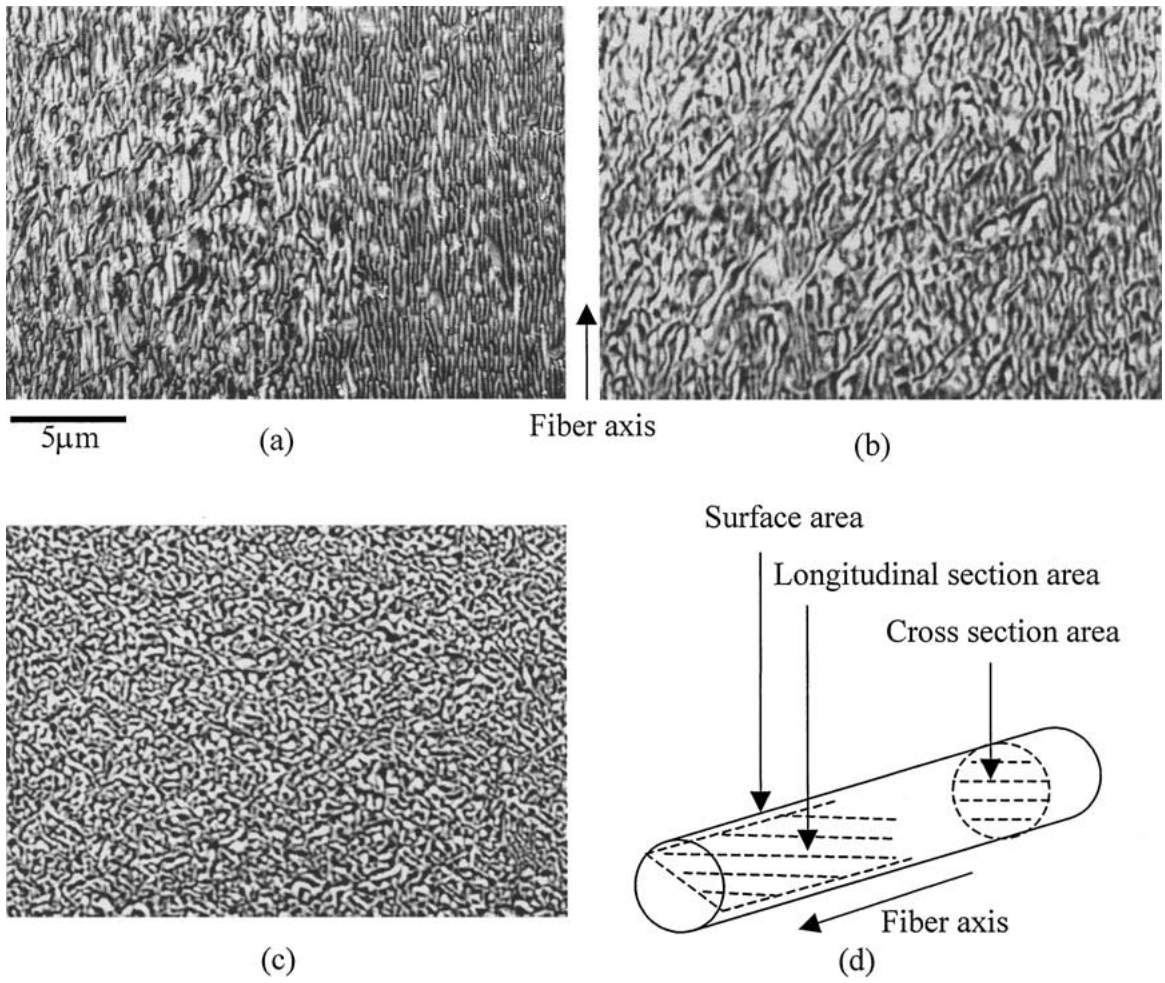

Figure 1 Microstructures of the $Y_3Al_5O_{12}/Al_2O_3$ eutectic fiber in the as-fabricated state (a) the surface area, (b) the longitudinal section area, (c) the cross section area, and (d) a schematic sketch illustrating the three different areas of the fiber.

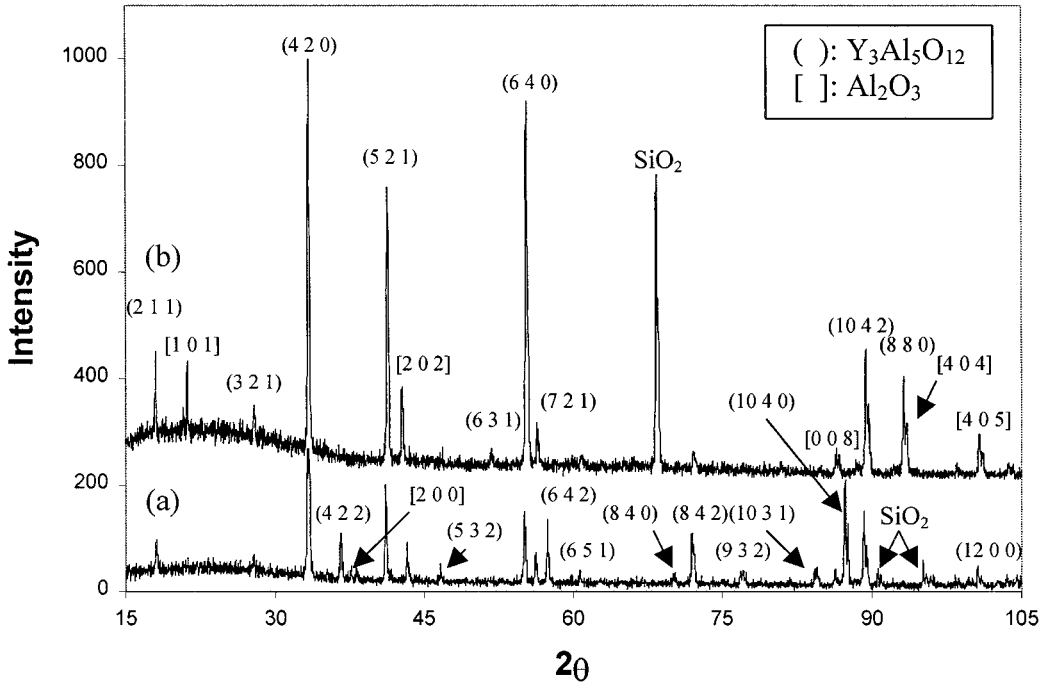

Figure 2 XRD patterns of the $Y_3Al_5O_{12}/Al_2O_3$ eutectic fiber before and after heat treatment at 1460°C for 200 hours.

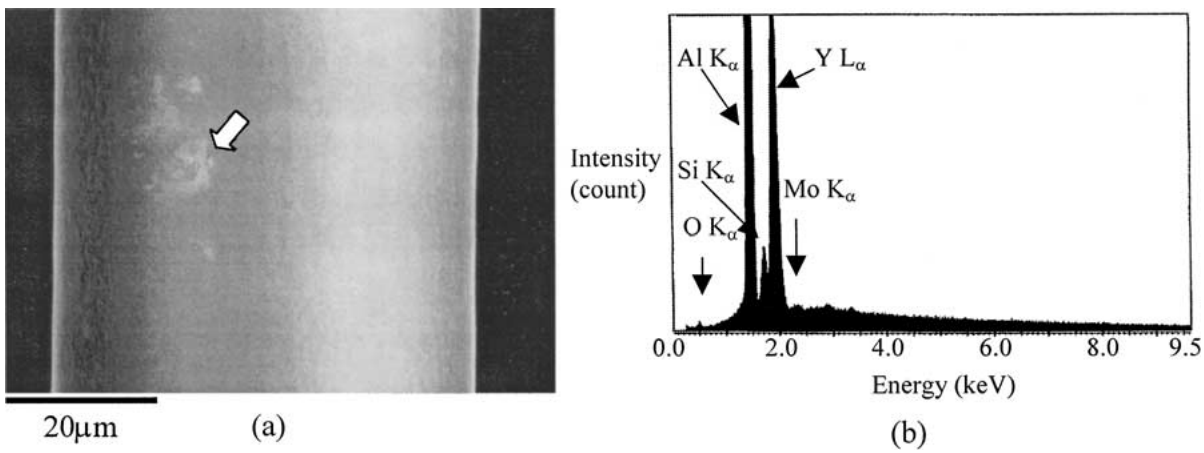

Figure 3 Impurities on the surface of the $Y_3Al_5O_{12}/Al_2O_3$ eutectic fiber in the as-fabricated state (a) the contaminated part on the surface of the fiber and (b) EDS result of the contaminated part on the surface of the fiber.

at 1460°C for 200 hours. The presence of SiO_2 peaks might be due to impurity contamination during fiber growth as shown in Fig. 3. A recent study by Matson and Hecht also reported that the composition of the impurity on the surface of the $Y_3Al_5O_{12}/Al_2O_3$ eutectic fiber was silicon [17].

After heat treatment at 1460°C for 100 hours and 200 hours in air, the thickness of $Y_3Al_5O_{12}$ and Al_2O_3 phases at the surface and the longitudinal section areas increased gradually as a function of heat treatment time as shown in Fig. 4. The coarsening of the lamellar structures both at the surface and the longitudinal section areas was clearly observed. The driving force for coarsening of the eutectic lamellar structures is believed to be the reduction of the interfacial energy (reductions in the total length of interface line between $Y_3Al_5O_{12}$ and Al_2O_3 phases in this study) through diffusion process [18, 19]. The change of lamellar spacing (λ) as a function of heat treating time is shown in Fig. 5. The lamellar spacing gradually increased with increasing heat treatment time. The lamellar spacing of the as-fabricated fiber at the longitudinal section area was measured to be 0.52 μm, and it increased to be 1.18 μm after heat treatment at 1460°C for 200 hours. However, the lamellar spacing at the surface area was increased from 0.40 μm to 2.61 μm after heat treatment at 1460°C for 200 hours. The increases of lamellar spacing at the surface and the longitudinal section areas were found to be 648% and 223%, respectively. The increase of lamellar spacing at the surface area at 1460°C for 200 hours is about 3 times larger than that at the longitudinal section area. The detailed mechanisms and kinetics of coarsening have been discussed by Park *et al.* [20].

3.2. Tensile strength

The tensile strengths of the $Y_3Al_5O_{12}/Al_2O_3$ eutectic fiber before and after heat treatment at 1460°C for 200 hours were measured as shown in Fig. 5. The

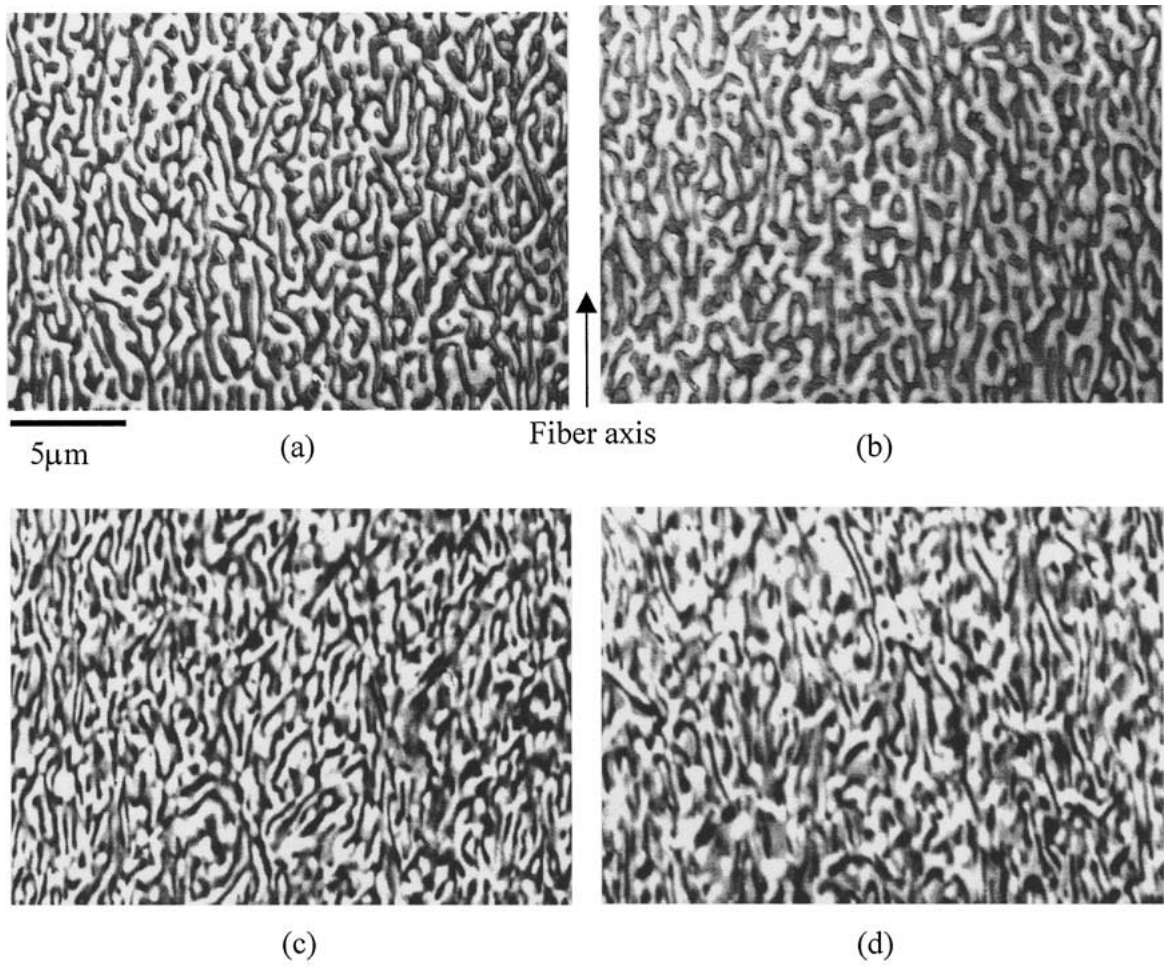

Figure 4 Microstructures of the $Y_3Al_5O_{12}/Al_2O_3$ eutectic fibers at the surface and the longitudinal section area after heat treatment at 1460°C in air (a) the surface area for 100 hours, (b) the surface area for 200 hours, (c) the longitudinal section area for 100 hours, and (d) the longitudinal section area for 200 hours.

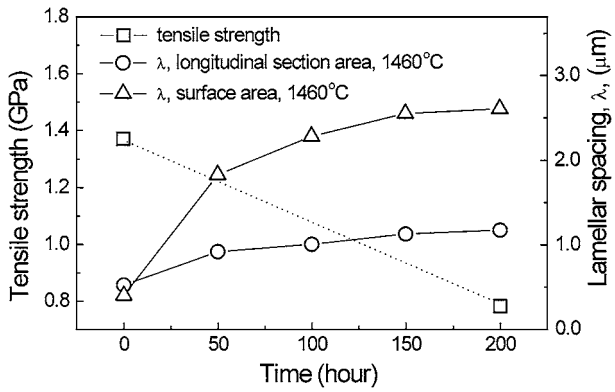

Figure 5 The changes of tensile strength and lamellar spacing as a function of heat treatment time at the surface area and the longitudinal section area.

TABLE I Tensile strengths of single crystal oxide fibers and oxide-oxide eutectic fibers

Fiber	Fiber diameter (μm)	Tensile strength (GPa)	Ref.	Comments
Al_2O_3	150	2.6	21	Single crystal *c*-axis fiber produced by Saphikon Inc.
	254	2.37–2.62	22	Single crystal *c*-axis fiber Produced by Saphikon Inc.
$Y_3Al_5O_{12}$	170	0.90	4	Single crystal YAG fiber
	240	1.07	4	Single crystal YAG fiber
$Y_3Al_5O_{12}/Al_2O_3$	125	1.93	9	Eutectic fiber grown by EFG (Saphikon Inc.)
$Al_2O_3/ZrO_2(Y_2O_3)$	125	1.20	23	Eutectic fiber grown by EFG (Saphikon Inc.)

average tensile strength decreased from 1.37 GPa to 0.78 GPa after heat treatment at 1460°C for 200 hours. The room temperature tensile strengths of single crystal alumina fibers were measured to be 2.4–2.6 GPa [21, 22]. Corman [4] reported the tensile strength values of 0.90–1.07 GPa for single crystal $Y_3Al_5O_{12}$ fiber. The tensile strength of the $Y_3Al_5O_{12}/Al_2O_3$ fiber in this study appeared to be in the range between that of single crystal alumina and single crystal $Y_3Al_5O_{12}$ as shown in Table I. Also, the $Y_3Al_5O_{12}/Al_2O_3$ fiber in this study exhibited a higher tensile strength to the EFG processed $Al_2O_3/ZrO_2(Y_2O_3)$ eutectic fiber [23]. The tensile strength distribution and Weibull's modulus of the as-fabricated and the heat-treated eutectic fibers are shown in Fig. 6. The results show the Weibull's modulus decreased from 11.2 for the as-fabricated fibers

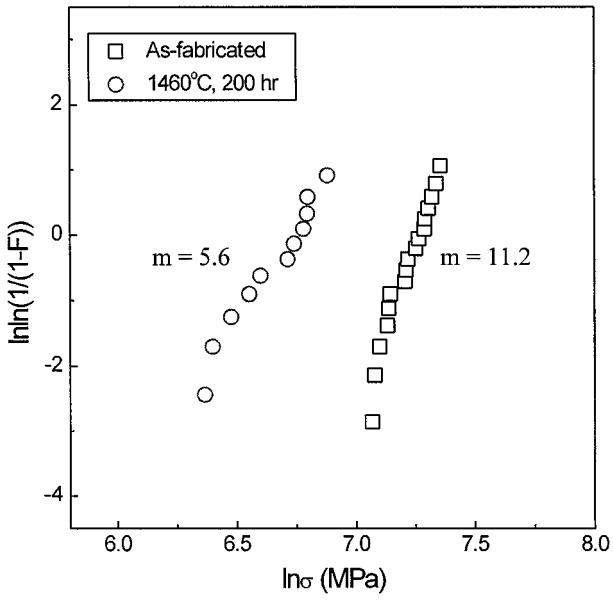

Figure 6 Tensile strength distribution and Weibull's modulus of the $Y_3Al_5O_{12}/Al_2O_3$ fiber before and after heat treatment at 1460°C for 200 hours in air.

to 5.6 for the heat-treated fibers. A recent study by Farmer *et al*. also reported that the tensile strength of the $Y_3Al_5O_{12}/Al_2O_3$ eutectic fibers grown by EFG technique decreased approximately 40% after annealing at 1400°C for 2 hours in flowing argon [10].

SEM fractographic analysis of the as-fabricated fibers indicated that fracture initiated at surface flaw. Microstructural examination also revealed that surface grooves at the intephase region between the $Y_3Al_5O_{12}$ and the Al_2O_3 phases were developed after heat treatment at 1460°C for 100 hours as shown in Fig. 7. The main driving force for the surface grooves induced by the heat treatment is believed to be the reduction of the interfacial free energy (reductions in the total surface areas between $Y_3Al_5O_{12}$ and Al_2O_3 interfaces) in the eutectic microstructures. It is evident that the coarsening rate of $Y_3Al_5O_{12}$ and Al_2O_3 phases at the surface of the fiber is much faster than that at the interior region (the longitudinal section area) of the fiber in Fig. 5. The different coarsening rate between the surface and the longitudinal section areas result from the difference in diffusion mechanisms. The coarsening at the surface area of the fiber can occur mainly through the surface diffusion rather than through the interphase boundary diffusion and volume diffusion. However, the coarsening at the interior area of the fiber will occur through the interphase boundary diffusion and the volume diffusion. It is well known that the rate of the surface diffusion is much faster than that of the interphase boundary diffusion and volume diffusion [24, 25]. The surface grooves at the surface of $Y_3Al_5O_{12}/Al_2O_3$ eutectic fiber is the obvious evidence that the coarsening at the surface of the fiber occurred through the surface diffusion mechanism. The migration of atoms near the interphase between the $Y_3Al_5O_{12}$ and Al_2O_3 phases moved to the convex side of a curved surface and developed the surface groove. The development of the surface grooves at the surface of a polycrystalline through the surface diffusion wherever a stationary grain boundary emerges to intersect the surface has been suggested [26, 27]. Tsoga *et al*. [28, 29] reported the grain boundary grooving on the polished surfaces of polycrystalline oxides (such as yttria-stabilized zirconia, calcia-stabilized zirconia and alumina) due to surface diffusion. A recent study by Jin *et al*. [30] also reported thermal grain boundary groove on the polished $SrTiO_3$ bicrystal after annealing at 1150–1400°C.

The grooves developed at the surface of the $Y_3Al_5O_{12}/Al_2O_3$ eutectic fiber after heat treatment resulted in increase of the surface roughness of the fiber as shown in Fig. 8. It is believed that the surface grooves acted as the stress concentration sites (which will cause the notch effect in $Y_3Al_5O_{12}/Al_2O_3$ eutectic fiber) during tensile test. Fig. 8b clearly shows the extensive development of the surface grooves at the surface of the fiber in which a fracture initiated.

3.3. Fracture toughness and crack propagation

The cracks produced by Vickers indenter in the $Y_3Al_5O_{12}/Al_2O_3$ eutectic fiber was assessed using stepwise polishing as shown in Fig. 9. Fig. 9a shows the Vickers indentation mark produced on the polished surface of the $Y_3Al_5O_{12}/Al_2O_3$ eutectic fiber. Two

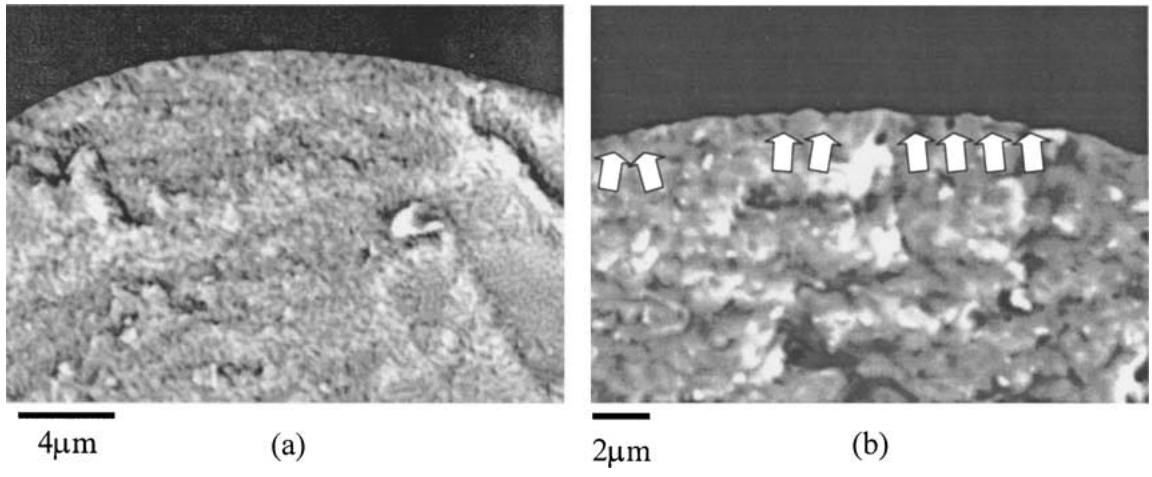

Figure 7 Surface grooves on the surface of the $Y_3Al_5O_{12}/Al_2O_3$ eutectic fiber before and after heat treatment (a) the as-fabricated state and (b) after heat treatment at 1460°C for 100 hours in air.

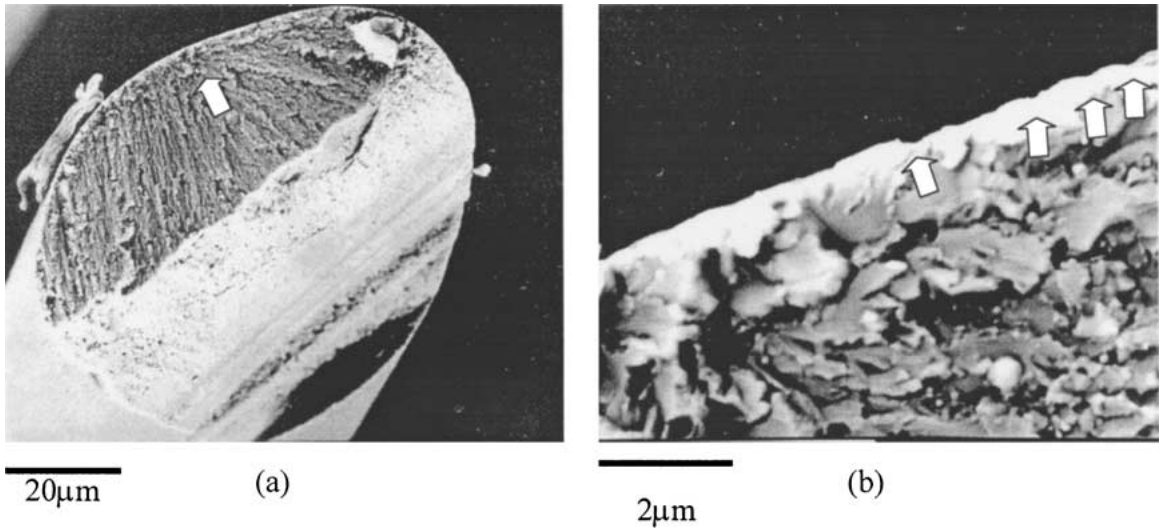

Figure 8 Surface grooves on the surface of the $Y_3Al_5O_{12}/Al_2O_3$ fiber after tensile test (the fiber was heat-treated at 1460°C for 200 hours in air before tensile test) (a) low magnification and (b) high magnification.

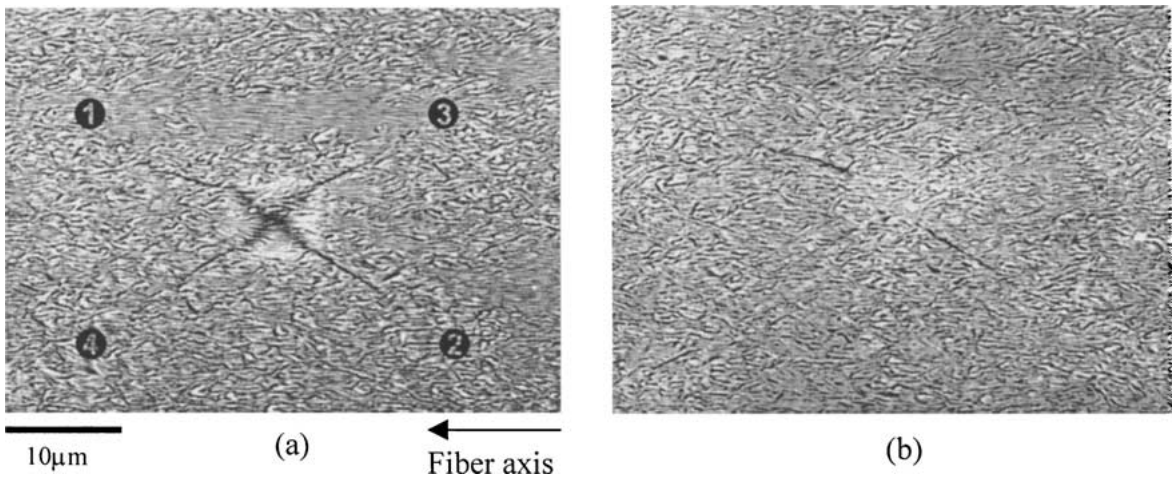

Figure 9 Vickers indentation marks showing Palmqvist crack type in the $Y_3Al_5O_{12}/Al_2O_3$ fiber (a) the original Vickers indentation mark produced on the polished surface of the fiber, (b) after 12 μm was removed from the original polished surface.

cracks (①, ②) in Fig. 9a are never interconnected each other after 12 μm from the original polished surface was removed. Also, two cracks (③, ④) in Fig. 9a are never interconnected each other. It is evident that the $Y_3Al_5O_{12}/Al_2O_3$ fiber exhibits the radial (Palmqvist) crack type with 100 g load.

The load dependence of indentation diagonal is often described by the so-called Meyer law [31],

$$P = C \cdot D^n \tag{1}$$

where P is the indentation load, D is the corresponding indentation diagonal, C is the load to make an unit size indentation, and n is a measure for the load dependence of the hardness and thus of the size effect. A typical Meyer's plot of the $Y_3Al_5O_{12}/Al_2O_3$ eutectic fibers is shown in Fig. 10. The measured n was 1.632 from the Meyer's plot and this value is typical in ceramics [31]. Hardness of the $Y_3Al_5O_{12}/Al_2O_3$ eutectic fiber was measured to be 20.43 GPa (1 N load). This value is very similar to the hardness of Al_2O_3 (about 20 GPa at 1 N load) [32] and $Y_3Al_5O_{12}$ (20.2 GPa at 1 N load) [31].

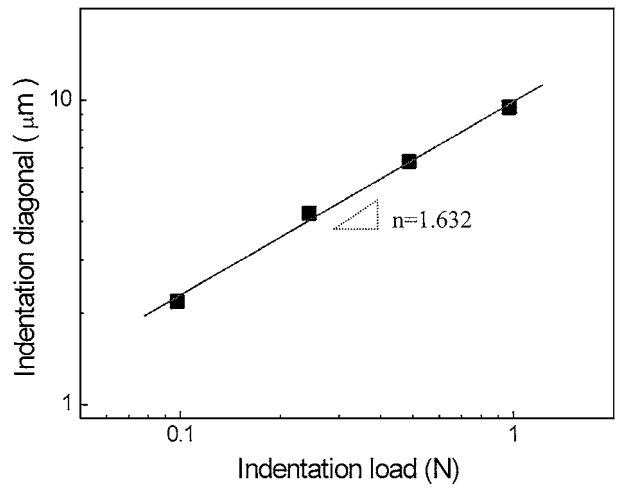

Figure 10 The changes of the indentation diagonal as a function of indentation load (Meyer plot).

The changes of Palmqvist crack length, a, as a function of indentation load in the $Y_3Al_5O_{12}/Al_2O_3$ eutectic fiber are shown in Fig. 11. The Palmqvist crack length linearly changed with the indentation load, P,

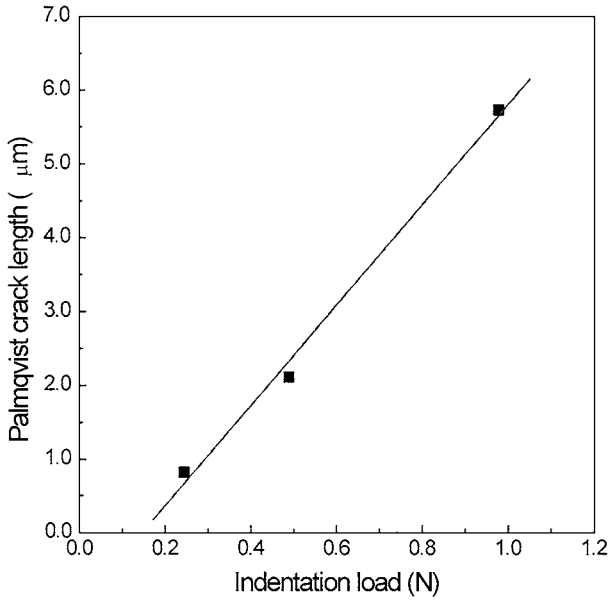

Figure 11 Load dependence of Palmqvist crack length in direction parallel to the fiber axis.

according to the following equation [33];

$$a = \frac{(P - P_0)}{4W} \tag{2}$$

where a is a Palmqvist crack length, P_0 is a threshold indentation load for crack initiation and W is a constant which is termed Palmqvist crack resistance [34]. Similar linear change in Palmqvist crack length versus the indentation load was also reported in glass-ceramic (Pyroceram 9606) [33].

The $Y_3Al_5O_{12}/Al_2O_3$ eutectic fiber exhibited an anisotropic crack propagation as shown in Fig. 12. The crack length in direction along the fiber axis is relatively longer compared to that in direction perpendicular to fiber axis in Fig. 12a. The crack cut through the lamellar structure without being deflected along the $Y_3Al_5O_{12}/Al_2O_3$ interfaces. This suggests that the bonding between $Y_3Al_5O_{12}$ and Al_2O_3 phases is strong. In order to investigate the anisotropy of crack propagation in different directions with respect to the fiber axis, the diamond Vickers indenter was rotated 45° with respect to the fiber axis as shown in Fig. 12d. In this case, the crack lengths are nearly identical in both directions. It is obvious that the $Y_3Al_5O_{12}/Al_2O_3$ eutectic fiber show the anisotropic crack propagation only in direction normal to the fiber axis. This suggests that the fracture resistance for crack propagating in direction perpendicular to the fiber axis is clearly better than that in direction parallel to the fiber axis. A study by Echigoya *et al.* also reported the anisotropic nature of the fracture toughness in a directionally solidified $Al_2O_3/ZrO_2(Y_2O_3)$ eutectics grown by a xenon lamp infrared heating furnace [35]. The $Y_3Al_5O_{12}/Al_2O_3$ eutectic fiber after heat treatment at 1460°C for 200 hours showed similar crack propagation behavior compared to the as-fabricated fiber as shown in Fig 12c. Apparently, coarsening of lamellar microstructure did not affect the crack propagation behavior.

The fracture toughness (K_{1C}) of $Y_3Al_5O_{12}/Al_2O_3$ eutectic fiber were measured by the indentation technique as shown in Table II. The fracture toughness (K_{1C}) was calculated using the following two equations [33, 36, 37];

$$K_{1C} = \beta \cdot (HW)^{1/2} \tag{3}$$

$$\left(\frac{K_{1C}}{H} \cdot \frac{\Phi}{a^{1/2}}\right)\left(\frac{H}{E \cdot \Phi}\right)^{2/5} = 0.035\left(\frac{l}{a}\right)^{-1/2} \tag{4}$$

where β is a non-dimensional constant dependent on the indenter geometry, H is the hardness, W is Palmqvist crack resistance, ϕ is the constraint factor ($\cong$3), a is the half-diagonal of the Vickers indent, E is the Young's modulus and l is Palmqvist crack length. Because the $Y_3Al_5O_{12}/Al_2O_3$ eutectic fiber showed the anisotropic behavior in fracture toughness (K_{1C}), a different Young's modulus should be used in Equation 4. Unfortunately the Young's modulus for the $Y_3Al_5O_{12}/Al_2O_3$ eutectic fiber is not available. In order to determine the Young's modulus for the directions parallel to the fiber axis ($E_\parallel$) and perpendicular to the fiber axis ($E_\perp$), Young's modulus for the two different directions to the fiber axis, $E_\parallel$ and $E_\perp$, were calculated by the approximate formula [38]

$$E_\parallel = E_{YAG}V_{YAG} + E_{alumina}V_{alumina} \tag{5}$$

$$E_\perp = \frac{E_{YAG} \cdot E_{alumina}}{E_{alumina} \cdot V_{YAG} + E_{YAG} \cdot V_{alumina}} \tag{6}$$

With [31, 39] reported Young's modulus of 290 GPa for $Y_3Al_5O_{12}$ and 400 GPa for Al_2O_3. The volume fractions of $Y_3Al_5O_{12}$ and Al_2O_3 phases in the $Y_3Al_5O_{12}/Al_2O_3$ eutectic fiber were measured to be 0.460 and 0.540, respectively, using the point count method [15]. Fracture toughness values of the $Y_3Al_5O_{12}/Al_2O_3$ eutectic fiber in direction along the fiber axis and in direction 45° with respect to the fiber axis were calculated to be 2.93 ± 0.83 MPa $\cdot$ m$^{1/2}$ and 2.88 ± 0.34 MPa $\cdot$ m$^{1/2}$, respectively, using the Equation 3 suggested by Shetty *et al.* [33]. The fracture toughness values for MgO-doped (250 ppm) $Y_3Al_5O_{12}$ and SiO_2-doped (500 ppm)

TABLE II Measurements of fracture toughness (K_{1C}) of $Y_3Al_5O_{12}/Al_2O_3$ eutectic fiber

	K_{1C} (MPa $\cdot$ m$^{1/2}$)					
	Eq. suggested by Shetty *et al.* [33]			Eq. suggested by Niihara *et al.* [37]		
	$\parallel$ to fiber axis	45° rotated to fiber axis	$\perp$ to fiber axis	$\parallel$ to fiber axis	45° rotated to fiber axis	$\perp$ to fiber axis
As-fabricated	2.93 ± 0.83	2.88 ± 0.34	5.78 ± 1.74	4.83 ± 1.36	4.75 ± 0.57	9.17 ± 2.78
1460°C/200 hr	2.88 ± 0.49	–	5.34 ± 1.79	4.79 ± 0.85	–	9.69 ± 4.06

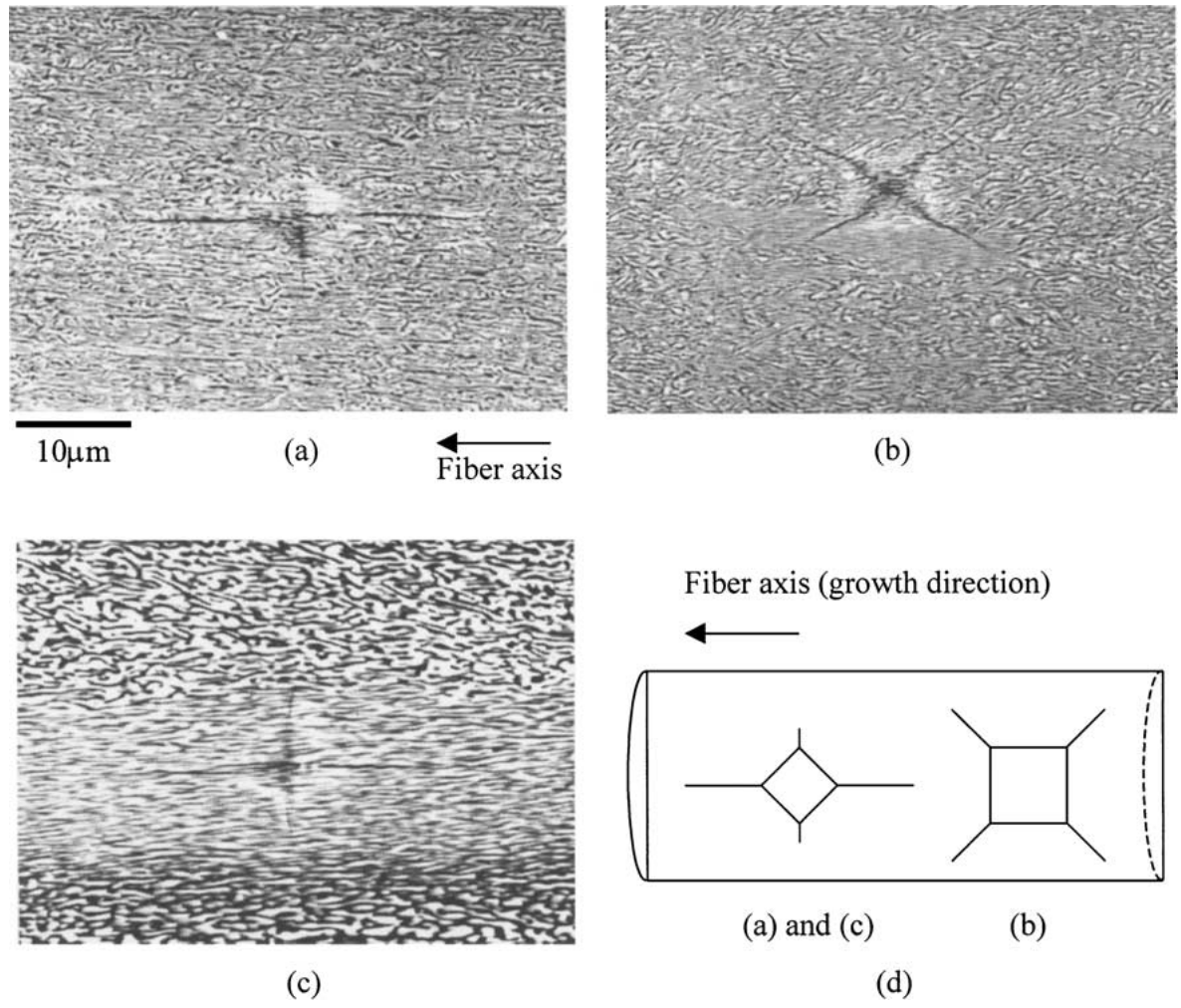

Figure 12 Cracking patterns of the $Y_3Al_5O_{12}/Al_2O_3$ eutectic fiber under the indentation load of 0.1 kg (a) the as-fabricated state, (b) the as-fabricated state, indenter rotated 45-degree with respect to fiber axis, (c) the heat-treated state at 1460°C for 200 hours, and (d) indenter setups with respect to the fiber axis.

$Y_3Al_5O_{12}$ ceramics were measured to be 1.87 $MPa \cdot m^{1/2}$ and 1.84 $MPa \cdot m^{1/2}$, respectively, using the three point bend test [31]. With [39] reported the fracture toughness value of 3.71 $MPa \cdot m^{1/2}$ for MgO-doped (5 ppm) Al_2O_3, using the three point bend test. Also, several investigations using different test methods have been reported that the fracture toughness values for Al_2O_3 were measured to be somewhere around 4 $MPa \cdot m^{1/2}$ [39]. Fracture toughness values in this study appeared to be in the range between the values for $Y_3Al_5O_{12}$ and Al_2O_3. However the fracture toughness values of the $Y_3Al_5O_{12}/Al_2O_3$ eutectic fiber in direction perpendicular to the fiber axis were calculated 5.78 ± 1.74 $MPa \cdot m^{1/2}$. The fracture resistance for crack propagation in direction perpendicular to the fiber axis is clearly better than that in direction parallel to the fiber axis for both the as-fabricated and heat-treated fiber.

4. Summary

The microstructure of the directionally solidified $Y_3Al_5O_{12}/Al_2O_3$ eutectic fiber grown by EFG technique consists of fine, well-aligned lamellar microstructures along the fiber axis: $Y_3Al_5O_{12}$ phases are distributed uniformly in Al_2O_3 phases. Significant coarsening of the fine lamellar structure of the $Y_3Al_5O_{12}/Al_2O_3$ eutectic fiber occurred after exposure at elevated temperature. The room temperature tensile strength after heat treatment decreased significantly due to the development of grooves on the surface.

It was found that the $Y_3Al_5O_{12}/Al_2O_3$ eutectic fiber showed the radial (Palmqvist) crack type under 100 g load. Also, the $Y_3Al_5O_{12}/Al_2O_3$ eutectic fiber exhibited an anisotropic crack propagation behavior. The coarsening of lamellar microstructure in the $Y_3Al_5O_{12}/Al_2O_3$ eutectic fiber did not affect the fracture toughness (K_{1C}) values. This is because the $Y_3Al_5O_{12}/Al_2O_3$ eutectic fiber still maintained the aligned lamellar microstructures after heat treatment.

References

1. S. A. NEWCOMB and R. E. TRESSLER, *J. Amer. Ceram. Soc.* **76**(10) (1993) 2505.
2. J. E. SHEEHAN, J. SIGALOVSKY, J. S. HAGGERTY and J. R. PORTER, *Ceram. Eng. Sci. Proc.* **14**(7/8) (1993) 660.
3. K. J. McCLELLAN, H. SAYIR, A. H. HEUER, A. SAYIR, J. HAGGERTY and J. SIGALOVSKY, *ibid.* **14**(7/8) (1993) 651.
4. G. S. CORMAN, in 94th Annual Meeting of the American Ceramic Society, Minneapolis, MN, April 12–16, 1992.
5. S. C. FARMER, A. SAYIR and P. O. DICKERSON, in *In Situ Composites: Science and Technology* (The Metallurgical Society, Warrendale, PA, 1993) p. 167.

6. E. L. COURTRIGHT, J. S. HAGGERTY and J. SIGALOVSKY, *Ceram. Eng. Sci. Proc.* **14**(7/8) (1993) 671.
7. H. E. BATES, *ibid.* **13**(7/8) (1992) 190.
8. T. MAH, T. A. PARTHASARATHY and M. D. PETRY, *ibid.* **14**(7/8) (1993) 622.
9. J.-M. YANG, S. M. JENG and S. CHANG, *J. Amer. Ceram. Soc.* **79**(5) (1996) 1218.
10. S. C. FARMER, A. SAYIR, P. O. DICKERSON and S. L. DRAPER, in 19th Annual Conference on Composites, Advanced Ceramics, Materials and Structures, Ceram. Eng. Sci. Proc., Vol. 16, No. 5, 969 (1995).
11. B. LAWN and R. WILSHAW, *J. Mater. Sci.* **10** (1975) 1049.
12. B. LAWN, "Fracture of Brittle Solids" (Cambridge University Press, Cambridge, U.K., 1993) Ch. 8.
13. D. TABOR, "Hardness of Metals" (Clarendon, Oxford, U.K., 1951).
14. H. E. LABELLE, JR., *Mat. Res. Bull.* **6** (1971) 581.
15. T. MAH, T. A. PARTHASARATHY and L. E. MATSON, *Ceram. Eng. Sci. Proc.* **11**(9/10) (1990) 1617.
16. E. E. UNDERWOOD, "Quantitative Stereology" (Addison-Wesley, Massachusetts, 1970).
17. L. E. MATSON and N. HECHT, *J. Euro. Ceram. Soc.* **19** (1999) 2487.
18. L. D. GRAHAM and R. W. KRAFT, *Trans. Met. Soc. AIME* **236** (1966) 94.
19. A. J. ARDELL, in "Computer-Aided Design of High-Temperature Materials," edited by Alexander Pechenik *et al.* (Oxford University Press, Oxford, 1999) p. 163.
20. D.-Y. PARK, J.-M. YANG and J. M. COLLINS *J. Amer. Ceram. Soc.*, in press.
21. S. NOURBAKHSH, W. H. RHEE, O. SAHIN and H. MARGOLIN, *Metall. Mater. Trans. A* **25A** (1994) 1259.
22. R. L. CRANE and R. E. TRESSLER, *J. Comp. Mater.* **5** (1971) 537.
23. J.-M. YANG and X. Q. ZHU, *Scrip. Mater.* **36**(9) (1997) 961.
24. K.-N. TU, J. W. MAYER and L. C. FELDMAN, "Electronic Thin Film Science for Electrical Engineers and Materials Scientists" (Macmillan, New York, 1992).
25. J. ASKILL, "Tracer Diffusion Data for Metals, Alloys and Simple Oxides" (IFI/Plenum, New York, 1970).
26. W. W. MULLINS, *J. Appl. Phys.* **28** (1957) 333.
27. *Idem.*, *Trans. Met. Soc. AIME* **218** (1960) 354.
28. A. TSOGA and P. NIKOLOPOULOS, *J. Amer. Ceram. Soc.* **77**(4) (1994) 954.
29. A. TSOGA, D. SOTIROPOULOU and P. NIKOLOPOULOS, *Mater. Sci. Forum* **207–209** (1996) 565.
30. M. JIN, E. SHIMADA and Y. IKUMA, *J. Mater. Res.* **14**(6) (1999) 2548.
31. G. DE WITH and J. E. D. PARREN, *Solid State Ionics* **16** (1985) 87.
32. D. J. CLINTON and R. MORRELL, *Brit. Ceram. Proc.* **34** (1984) 113.
33. D. K. SHETTY, A. R. ROSENFIELD and W. H. DUCKWORTH, *J. Amer. Ceram. Soc.* **68**(10) (1985) C-282.
34. H. E. EXNER, *Trans. Met. Soc. AIME* **245** (1969) 677.
35. J. ECHIGOYA, Y. TAKABAYASHI and H. SUTO, *J. Mater. Sci. Lett.* **5** (1986) 153.
36. K. NIIHARA, *ibid.* **2** (1983) 221.
37. K. NIIHARA, R. MORENA and D. P. H. HASSELMAN, *ibid.* **1** (1982) 13.
38. R. W. DAVIDGE, "Mechanical Behaviour of Ceramics" Cambridge Solid State Science Series (Cambridge University Press, Cambridge, 1980) p. 24.
39. G. DE WITH, *J. Mater. Sci.* **19** (1984) 2195.

Received 28 September 2000
and accepted 31 May 2001